Microstructure evolution in a 3%Co modified P911 heat resistant steel under tempering and creep conditions

A. Kipelova [a,*], R. Kaibyshev [a], A. Belyakov [a], D. Molodov [b]

[a] Belgorod State University, Pobeda 85, Belgorod 308015, Russia
[b] Institute of Physical Metallurgy and Metal Physics, RWTH Aachen University, 52056 Aachen, Germany

ABSTRACT

Microstructure evolution was studied in a 3%Co modified P911 heat resistant steel during creep tests at 873 and 923 K to failure, which occurred in 4103 and 4743 h, respectively. The tempered martensite lath structure consisted of packets, blocks and laths. The average spacing of high-angle boundaries and the mean transverse lath size were about 1.9 μm and 360 nm, respectively. Various second phase particles precipitated upon tempering. Fine M(C, N) carbonitrides with an average size of about 30 nm were homogeneously distributed throughout the tempered martensite laths, while relatively coarse $M_{23}C_6$ carbide particles (average size 120 nm) were located at internal boundaries. The tempered martensite lath structure was rather stable upon aging for about 4×10^3 h. The boundary precipitates of $M_{23}C_6$ and Laves phases, which appeared during creep tests, exerted a high pinning pressure on low-angle lath boundaries and high-angle packet/block boundaries. The growth of martensite structural elements during the tests correlated with the coarsening of second phase particles. Quantitative relations of pinning and driving pressures for low- and high-angle boundaries are discussed.

1. Introduction

High chromium martensitic steels are widely used as heat resistant structural materials. One of the most efficient applications of these steels is associated with the manufacturing of components for advanced power plants [1–3]. The service properties of martensitic steels are achieved by a complex alloying that provides solution and dispersion strengthening. The creep resistance of martensitic steels depends on the stability of their tempered microstructure at elevated temperatures [4–7]. The main structural parameters of the steels after appropriate heat treatment include sizes of prior austenite grains, packets, blocks, and laths [6–9]. All structural elements of tempered martensite must keep their original size over a long time in order to provide suitable service properties. The most effective mechanism for microstructure stabilization is the pinning of high-angle grain boundaries and low-angle dislocation boundaries by fine particle dispersions.

The tempered martensite lath structure (TMLS) of advanced heat resistant steels contains a number of second phase particles. Among those are fine particles of $M_{23}C_6$, which precipitate mainly at internal boundaries including lath boundaries, and homogeneously distributed fine MX carbonitrides [9,10]. After rather long aging and/or creep, relatively large particles of Laves phase appear within TMLS [5,7]. All second phase particles play a role as effective pinning agents to prevent microstructural coarsening during a long period of service life. The coarsening of second phase particles and the growth of martensite laths during service time may result in the degradation of creep resistance and may cause failure of load-bearing units. Therefore, studies on the stability of TMLS against coarsening at elevated temperatures are of great practical importance. The aim of the present work is to examine the microstructure of an advanced Co-bearing P911-type steel after tempering and creep tests. The study is particularly focused on the effect of second phase particles on microstructure stabilization and the evaluation of pinning and driving pressures for growth of structural elements in TMLS.

2. Experimental procedure

A 3%Co modified P911-type steel (0.13%C, 8.6%Cr, 3.2%Co, 1.2%W, 0.9%Mo, 0.2%V, 0.1%Cu, 0.07%Nb, 0.06%Si, 0.05%Ni, 0.04%N, 0.02%Mn, 0.005%B, all in mass%, and the balance Fe) was used as a representative of an advanced martensitic creep resistant steels. The ingot was hot forged at 1373 K to square bar of 25 mm × 25 mm. Then, the steel was austenitized at 1323 K for 0.5 h followed by air cooling and tempered at 1023 K for 3 h. Specimens of 10 mm gauge diameter and 50 mm gauge length were used for the creep tests. The creep tests were carried out at 873 and 923 K with initial stresses

* Corresponding author. Tel.: +7 4722 585457; fax: +7 4722 585417.
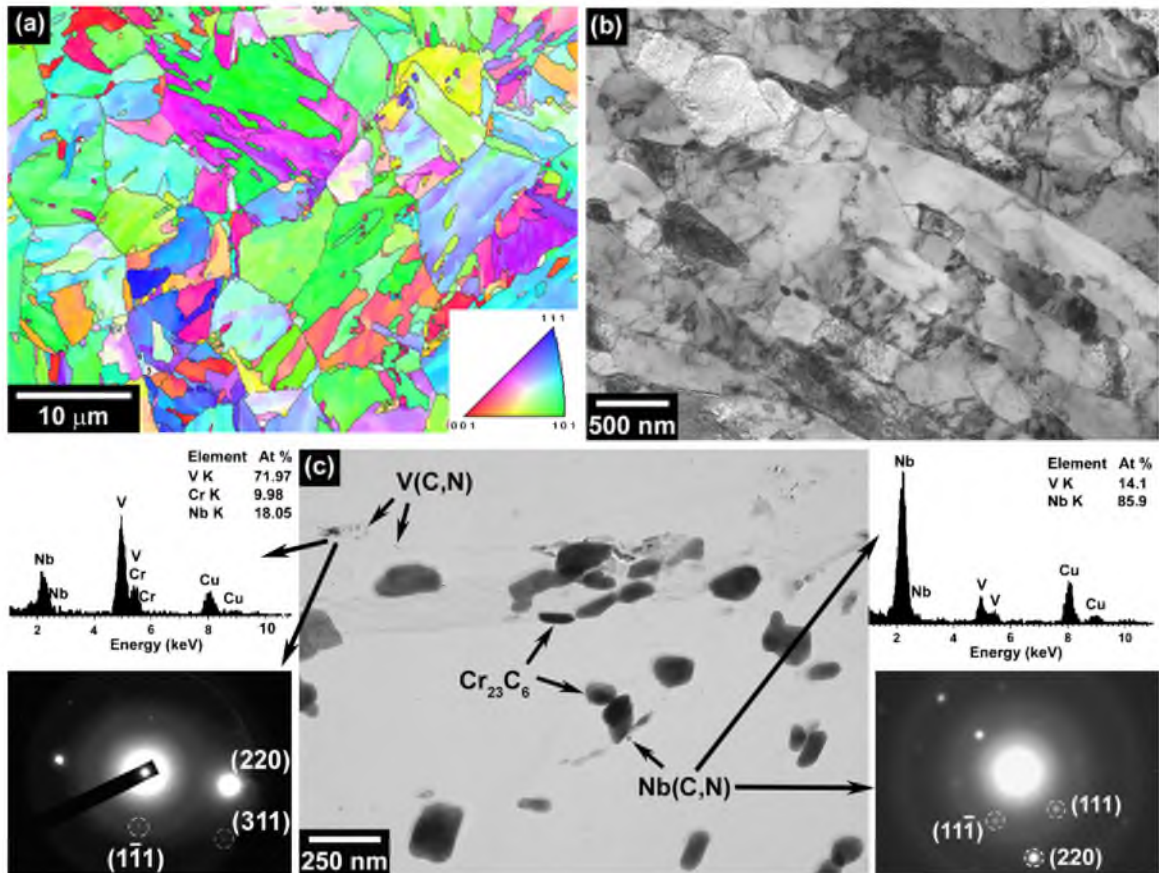   E-mail address: a.kipelova@gmail.com (A. Kipelova).

Fig. 1. TMLS in the 3%Co modified P911 steel; OIM micrograph showing the inverse pole figure for normal direction (a), TEM bright field image of lath substructure (b), second phase precipitates revealed by extraction replica (c).

of 200 and 120 MPa, respectively, up to rupture, which occurred in about 4.5×10^3 h under the both conditions.

The microstructural investigations were carried out by using a JEM-2100 transmission electron microscope (TEM) operating at 200 kV that was equipped with an INCA energy-dispersive X-ray spectrometer (EDS) and a Quanta 600 FEG scanning electron microscope incorporating an orientation imaging microscopy (OIM) system. The aged and crept microstructures were studied on longitudinal sections of tested specimens in the grip and neck (1.5 mm away from the fracture surface) portions, respectively. The TEM foils were prepared by double jet electro-polishing using a 10% solution of perchloric acid in glacial acetic acid. The same solution was used for OIM samples. Extraction replicas for the microchemical analysis of precipitates were prepared by the evaporation of carbon onto a polished and etched sample surface followed by dissolution of the metallic matrix in a 10% HCl with ethanol at a voltage of 2 V. The OIM maps of dimension of 50 μm × 50 μm were obtained under the following conditions: accelerating voltage of 20 kV, beam current of 18 nA, working distance of 10 mm, step size of 40 nm. The grain sizes were derived from OIM images as average distance between boundaries with misorientations above 15° as a critical value separating low- and high-angle boundaries. The lath/subgrain sizes were measured on TEM micrographs by the linear intercept method, counting all clearly defined (sub)boundaries. The "longitudinal" and "transverse" lath sizes used in this paper actually mean the long and short intercepts, respectively. At least 10 TEM bright field images under conditions of strong scattering from planes of {0 0 2}, {0 1 3}, or {2 2 2} were used for evaluation of dislocation density in lath/subgrain interiors. The dislocation density was estimated by counting individual dislocations crossing the thin foil surface [11]. The second phase particles were identified by

both chemical analysis and selected area diffraction. At least 250 particles were analyzed for each data point. Equilibrium volume fraction of phases at 873–1023 K was calculated with the software ThermoCalc using the TCFE4 database.

3. Results

3.1. Tempered microstructures

Typical OIM and TEM micrographs of the TMLS in the 3%Co modified P911 steel are shown in Fig. 1 along with a detailed image of second phase precipitates revealed by extraction replica. The prior austenite grains with an average size of about 14 μm are subdivided by high-angle packet/block boundaries and low-angle lath boundaries (Fig. 1a and b). The mean distance between high-angle boundaries (HABs) and the transverse lath size are about 1.9 μm and 360 nm, respectively. The lath interiors are characterized by a rather high dislocation density of about 6×10^{14} m^{-2}.

Mainly two types of precipitates, *i.e.* MX-type and M$_{23}$C$_6$-type carbides, were observed within the TMLS (Fig. 1c). The MX particles including plate-like V(C, N) and spherical Nb(C, N) had an average size of about 30 nm. The M$_{23}$C$_6$ particles were somewhat elongated; and their average size was about 120 nm. The fine MX particles were homogeneously distributed throughout the TMLS. On the other hand, almost all M$_{23}$C$_6$-type carbides were located at internal boundaries, *i.e.* prior austenite, packet, block and lath boundaries. It is stressed that the volume fractions of M$_{23}$C$_6$ particles precipitated at different kinds of boundaries were not the same. The density of these particles located at HABs of prior austenite grains/packets/blocks was nearly twice as high as that of the carbides situated at low-angle lath boundaries. The quantitative

Table 1
Some microstructural parameters for the 3%Co modified P911 steel after tempering at 1023 K.

| Spacing of HABs (µm)	Transverse/longitudinal lath size (nm)	Dislocation density, $\times 10^{14}$ (m^{-2})	Mean particle size (nm)		Particle volume fraction (%)	
			MX	M$_{23}$C$_6$	MX	M$_{23}$C$_6$
1.9	$360 \pm 45/3160 \pm 400$	6.2 ± 1.7	30 ± 2	118 ± 3	0.25	2.5

structural parameters of the tempered martensite in the 3%Co modified P911 steel are summarized in Table 1. Note here, the volume fractions of second phase particles were calculated by Thermo-Calc. The sizes of second phase particles revealed in the modified P911 + 3%Co steel after conventional heat treatment are in line with other studies on 9–12%Cr creep resistant steels that reported the ranges of 15–35 nm for MX size and of 90–140 nm [2,12–14].

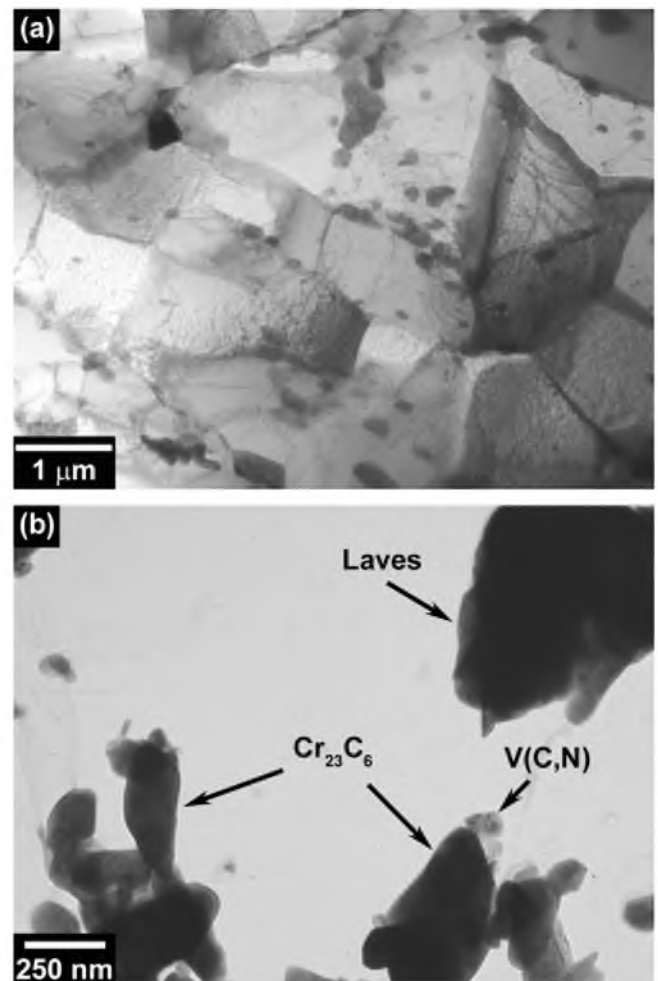### 3.2. Microstructures after creep test

Typical microstructures that evolved in the grip portions of samples subjected to creep tests for about 4×10^3 h are shown in Fig. 2. Generally, the microstructures in the grip portions looked similar to the initial TMLS in spite of the rather long time exposure to elevated temperatures. The structural changes were characterized by a small-scale growth of laths and structural elements outlined by HABs that took place concurrently with a slight coarsening of second phase particles. Depending on temperature, the transverse lath size enlarged from 360 nm to about 450–500 nm during the creep tests, whereas the spacing of HABs increased from 1.9 nm to

2.2–2.3 µm. The MX and M$_{23}$C$_6$ particles in the grip portions of the crept samples did not significantly coarsen during the tests. Major changes in the phase composition were associated with the appearance of relatively large Laves phase particles with an average size of 180 and 260 nm after testing at 873 and 923 K, respectively. Almost all Laves phase particles (about 90%) precipitated at HABs.

In contrast to the grip portions, the crept microstructures that developed in the vicinity of the fracture surfaces were quite different from the TMLS (Fig. 3). It should be noted that the reductions in area reached about 80% and 60% in the samples tested at 873 and 923 K, respectively; and the neck portions in the both samples spread over 20 mm along the tensile axes. Qualitatively, the original TMLS lost its lath morphology in the sample parts close to the neck, where large plastic strains occurred. The crept microstructures that developed in the neck portions looked like ordinary hot worked microstructures and were composed of subgrains elongated in plastic flow direction, the size of which remarkably exceeded the size of the original laths. The transverse subgrain sizes were about 660 and 1300 nm in the neck portions after creep
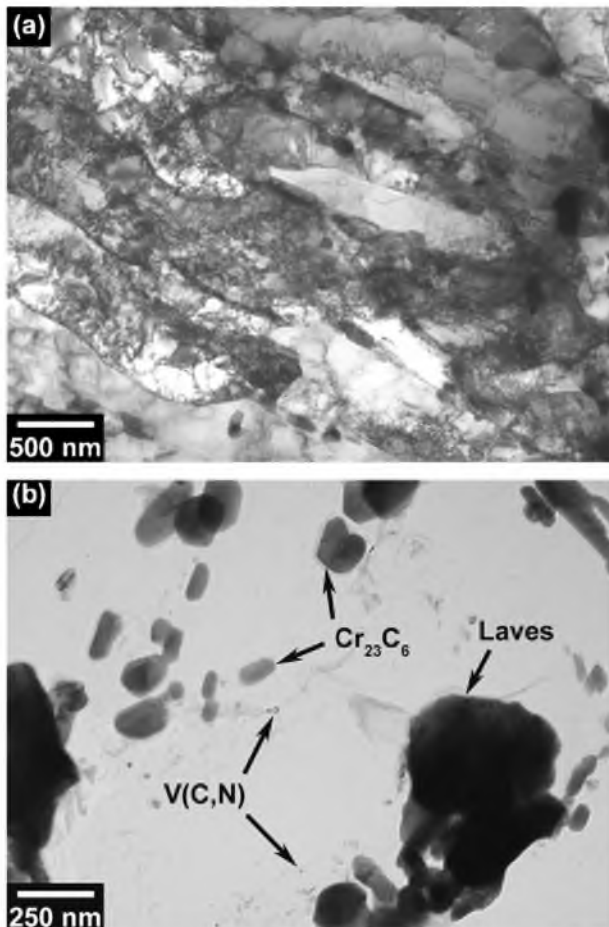
Fig. 2. Microstructure of the 3%Co modified P911 steel in grip portion of specimen crept at 923 K; TEM image of lath substructure (a), second phase particles (b).

Fig. 3. Microstructure of the 3%Co modified P911 steel in neck portion after creep test at 923 K; deformation substructure (a) and second phase particles (b).

Table 2
Microstructural parameters of the 3%Co modified P911 steel after creep tests at 873 and 923 K.

Structural parameters		Creep at 873 K, under 200 MPa, for 4103 h		Creep at 923 K, under 120 MPa, for 4743 h	
		Grip portion	Neck portion	Grip portion	Neck portion
Spacing of HABs (μm)		2.2 ± 0.3	1.6 ± 0.2	2.3 ± 0.3	3.9 ± 0.5
Longitudinal lath size (nm)		3230 ± 410	3350 ± 430	3615 ± 460	4400 ± 560
Transverse lath size (nm)		460 ± 60	660 ± 85	505 ± 65	1290 ± 165
Dislocation density, $\times 10^{14}$ (m^{-2})		5.3 ± 0.9	1.7 ± 0.3	2.9 ± 0.4	0.5 ± 0.1
Particle size (nm)	MX	39 ± 2	37 ± 3	48 ± 4	62 ± 4
	$M_{23}C_6$	100 ± 5	155 ± 10	125 ± 4	214 ± 16
	Laves	180 ± 4	170 ± 4	260 ± 7	265 ± 9
Particle volume fraction (%)	MX	0.23	0.23	0.23	0.23
	$M_{23}C_6$	2.5	2.5	2.5	2.5
	Laves	1.7	1.7	1.2	1.2

at 873 and 923 K, respectively. The increase in the size of the substructural elements clearly correlate with a decrease of the dislocation density from 6.2×10^{14} to 1.7×10^{14} m^{-2} at 873 K and 0.5×10^{14} m^{-2} at 923 K. It is noted that a remarkable increase in the spacing of HABs was observed only at 923 K. The phase changes in the neck portions were characterized by a coarsening of MX and $M_{23}C_6$ second phase particles as well as the development of Laves phases; and the coarsening kinetics quickened with temperature.

The results of structural investigations revealed that TMLS was rather stable during the annealing/aging, whereas hot working leads to transformation of the TMLS to a conventional deformation microstructure. The structural parameters that quantify the 3%Co modified P911 steel in the grip and neck portions are listed in Table 2. Commonly, the size of second phase particles increases with testing temperature. Different precipitates, however, demonstrated different coarsening rates in the grip and neck portions. The sizes of MX in the grip and neck portions were almost the same and depended only on the testing temperature. It should be noted that coarsening of MX precipitates during the tests and, in particular, almost twofold increase in their size after creep test at 923 K correlates well with other studies on particle coarsening in high chromium martensitic creep resistant steels [14,15]. The MX particles were shown essentially stable against coarsening at temperatures below about 873 K, while creep at higher temperatures was accompanied with relatively fast growth of such carbonitrides, *i.e.* their size was doubled in about 5×10^3 h at 923 K [2,14–16]. Also, the Laves phases precipitated with the same dimensions throughout the crept specimens. Both MX and Laves phase particles in the samples subjected to creep at 923 K were about 1.5 times larger than those tested at 873 K. On the other hand, the coarsening rate of $M_{23}C_6$ particles in the neck portions was much higher than in the grip sections. The size of $M_{23}C_6$ particles in the grip portions remained almost unchanged during the creep tests irrespective of temperature, while the neck portions were characterized by significant carbide coarsening. Almost the same coarsening behaviour of $M_{23}C_6$-type particles was reported for similar creep resistant steels [2,12,14–17]. Namely, the particles were characterized by a very slow coarsening rate at temperatures of $T \leq 873$ K, when their size remained at the level of 100 nm after long-term creep for more than 10^4 h, whereas increase in creep temperature to 923 K led an average particle size to about 200 nm.

4. Discussion

4.1. Pinning and driving pressures for lath/grain growth

The equilibrium size of the microstructural elements should reflect the balance between the driving and pinning pressures for grain/subgrain growth. The driving pressure results from the stored free energy, which is associated with any structural defect like grain/subgrain boundaries, lattice dislocations, etc., and can be released by the migration of grain/subgrain boundaries during annealing at elevated temperatures. In multiphase systems, boundary/subboundary motion is retarded by pinning forces arising from second phase particles. As originally proposed by Zener [18], the pinning pressure P_Z due to homogeneously distributed particles with size d and volume fraction F_V, acting on a boundary with energy per unit area γ can be derived [18] as:

$$P_Z = \frac{3\gamma F_V}{d} \qquad (1)$$

This equation can be used to evaluate the pinning pressure exerted by randomly distributed MX-type particles. The particles of $M_{23}C_6$ and Laves phases are located at various boundaries including lath boundaries. Taking the martensite lath as a prism with dimension of $l_0 \times L_1 \times L_3$, where l_0, L_1, and L_3 are the lath thickness, length, and width, respectively, the pinning pressure acting on the large side of the prism from the particles on the boundary reads [19]:

$$P_L = \frac{3\gamma l_0 F_V}{d^2} \qquad (2)$$

Here, F_V and d are volume fraction and size of the particles, respectively, precipitated at lath boundaries. The calculated pinning forces stabilizing the martensite lath boundaries by homogeneously distributed MX particles and boundary precipitations of $M_{23}C_6$ and Laves phases are presented in Table 3. The surface energy of a lath boundary was calculated from the Read and Shockley equation, $\gamma = Gb\theta(A - \ln\theta)/4\pi(1 - v)$, where G is the shear modulus, b is the Burgers vector, v is the Poisson ratio, and the term $A = 0.45$ [20], taking the misorientation angle (θ) of 1 degree. Since, the number of $M_{23}C_6$ phase particles per unit area of HAB is about double that those located at lath boundaries, the lath boundary spacing is approximately 1/5 of HAB spacing, and only 10% of Laves phase particles are at the lath boundaries, the equilibrium volume fractions of the $M_{23}C_6$ and Laves phase particles were multiplied by factors

Table 3
Pinning pressures from MX, $M_{23}C_6$ and Laves phases, stabilizing the martensite laths in the 3%Co modified P911 steel during creep at 873 and 923 K.

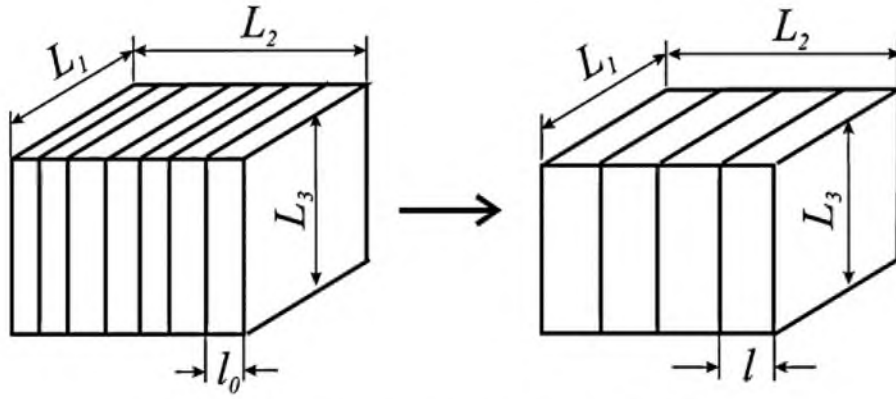| Pinning pressure	Creep at 873 K, under 200 MPa, for 4103 h		Creep at 923 K, under 120 MPa, for 4743 h	
	Grip portion	Neck portion	Grip portion	Neck portion
P_Z by MX (MPa)	0.05	0.05	0.03	0.03
P_L by $M_{23}C_6$ (MPa)	0.50	0.21	0.27	0.09
P_L by Laves phases (MPa)	0.02	0.02	0.01	0.01

Fig. 4. Schematic illustration for evaluation of driving force for lath growth.

of 0.67 and 0.1, respectively, to account for the difference in precipitate volume fractions at high-angle and lath boundaries. As seen in Table 3, the pinning by MX particles and Laves phases is negligibly small compared to $M_{23}C_6$ particles located at lath boundaries. The pinning pressure acting on lath boundaries from $M_{23}C_6$ particles is 3–10 times higher than the pressure exerted by homogeneously distributed particles.

Commonly, the driving pressure for grain/subgrain growth depends linearly on the boundary energy [18,19]. Considering an increase in the transverse lath size from l_0 to l (Fig. 4), the driving pressure P_B for lath growth that resulted from a decreasing lath boundary energy can be expressed as:

$$P_B = \gamma \left(\frac{1}{l_0} - \frac{1}{l} \right) \tag{3}$$

The TMLS is characterized by a somewhat increased dislocation density in the lath interior. Therefore, a decreasing dislocation density during the lath growth can provide an additional driving pressure P_d, which is directly proportional to a change of dislocation density $\Delta\rho$. Assuming that a moving lath boundary leaves a dislocation-free volume behind, $\Delta\rho = \rho_0 - N/S$, where ρ_0 is the initial dislocation density, N is the number of dislocations passing the lath cross section (invariant during lath growth), and S is the lath cross section (increases with increasing l). Then P_d can be evaluated from the following equation [19,21,22]:

$$P_d = 0.5Gb^2 \, \Delta\rho = 0.5Gb^2\rho_0 \left(1 - \frac{l_0}{l} \right) \tag{4}$$

where G and b are shear modulus and Burgers vector, respectively.

Lath growth can be expected to occur when the driving pressure exceeds the pinning force, *i.e.* $(P_B + P_d) > (P_Z + P_L)$. Combining Eqs. (1)–(4), the transverse lath size (l) corresponding to the balance of driving and pinning pressures can be obtained as a function of lath boundary energy, which, in turn, depends on misorientation angle. Fig. 5 depicts the lath size at which the driving and pinning pressures are equal in magnitude, as estimated from the experimental data in Tables 1 and 2.

The tempered martensite lath structure should be stable if the evaluated critical lath size is significantly larger than observed in the initial tempered state. It is seen in Fig. 5 that a slight increase in the size of martensite laths to about 400 nm results in the dominance of the driving pressures over the pinning ones in the neck portions of the samples. Therefore, a remarkable lath growth is expected in the neck portions, especially in the sample tested at 923 K, that clearly corresponds to the experimental observations. The lath size measured in the neck portions exceeded the size calculated from the balance condition (*cf.* Table 2 and Fig. 5). It should also be noted that the neck portions experienced large plastic strains during tertiary creep owing to the localization of

plastic flow. Therefore, the microstructure evolution in the neck portions of fractured specimens was affected by plastic deformation and may not reflect a static equilibrium between pinning and driving forces. Substructural parameters such as subgrain size and dislocation density that evolved under conditions of hot working are commonly expressed by power law functions of the flow stress [19,23–25]. A subgrain size exponent of −1 and a dislocation density exponent of 0.5 were reported in numerous studies. The relationships between subgrain size and dislocation density in the neck portions revealed in the present work (Table 2) obey the common expressions for deformation substructures.

On the other hand, the lath sizes for grip portions in Fig. 5 are considerably larger than the size of the tempered laths. This suggests that the lath structure can be effectively stabilized due to the sufficiently strong pinning pressures. However, for lath boundaries with very low misorientation angles (less than about 0.5°) an increase in the lath size up to about 400 nm (Fig. 5) results in such a decrease of the free energy that the effective driving forces can exceed the pinning forces exerted by the particles and, therefore, lath growth can occur due to migration of these very low angle lath boundaries. Thus, as observed in experiment, an increase of the lath
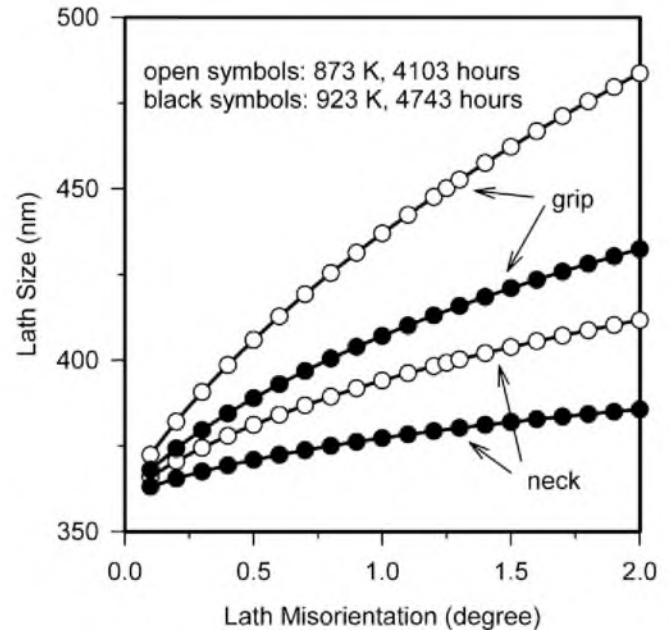

Fig. 5. Effect of misorientation angle on lath growth in the 3%Co modified P911 steel during creep at 873 and 923 K. The pinning and driving pressures were evaluated by Eqs. (1) and (2) and Eqs. (3) and (4), respectively.
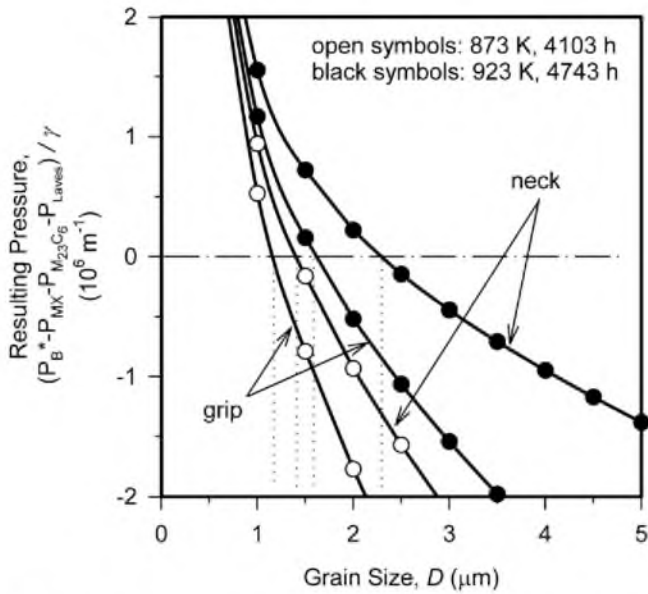
Fig. 6. Effect of grain size on driving pressure for grain growth in the 3%Co modified P911 steel during creep at 873 and 923 K.

size in the grip portions of crept specimens very likely resulted from the disappearance of individual low-angle lath boundaries which merged during the tests.

The driving pressure for grain growth that originated from the boundary surface energy is directly proportional to the ratio of the boundary energy to the radius of boundary curvature [11]. Taking the curvature radius as half of the grain size D, the driving pressure can be expressed as:

$$P_B^* = \frac{2\gamma}{D} \tag{5}$$

In six decades since the appearance of Smith's paper many attempts were made to derive quantitative expression for the driving pressure, taking into account some heterogeneity in the distributions of particle and grain sizes. Actually, almost all the treatments can be brought to a form of Eq. (5) with an additional factor of 0.1–0.5 [19,26–28]. TMLS is characterized by non-equilibrium triple junctions of HABs. Thus, it seems reasonable to use relatively large values of driving pressure predicted by Eq. (5) when considering grain growth.

Fig. 6 depicts the variation of the resulting pressure for grain growth normalized by the boundary energy versus the grain size. The pinning pressures due to MX particles were evaluated by Eq. (1) and those from $M_{23}C_6$ and Laves phases were estimated according to Eq. (2) taking the grain size instead of the lath size. The grain sizes obtained from the balance condition in Fig. 6 are somewhat smaller than the experimentally measured sizes. Therefore, the utilized approach allows only a rough evaluation of equilibrium grain size. However, as seen in Fig. 6, the driving pressure for grain growth rapidly increases with a decrease of the grain size, especially in the neck portions, where the second phase particles coarsen faster. Therefore, the increase of the average grain size can be associated with the accelerated shrinkage of fine grains, the size of which is below 1.5–2.0 μm.

Once the moving boundaries detached from the boundary particles, the pinning pressures of both the $M_{23}C_6$ and Laves phases correspond to those exerted by randomly distributed particles. Then, an equilibrium grain size can be evaluated by a simple combination of Eqs. (1) and (5). Utilizing the experimental data for the size and volume fractions of the various particles (Table 2), equilibrium grain sizes of 1.7 and 2.3 μm were calculated for the grip

portions of specimens tested at 873 and 923 K, respectively. Larger particle sizes in the neck portions resulted in larger equilibrium grain sizes, i.e. 2.1 μm at 873 K and 3.3 μm at 923 K. The calculated grain sizes were in line with experimental observations in spite of the simplified approach for estimating the resulting pressure.

4.2. Phase composition and stability of TMLS

As seen in Table 3, the calculated pinning force by MX carbonitrides, P_Z, slightly decreases with an increase of temperature and does not depend on deformation. In contrast, an increase of temperature from 873 to 923 K leads to a decrease of drag forces by $M_{23}C_6$ carbides and Laves phases by factors of about 2. In addition, the pinning pressure associated with the $M_{23}C_6$ carbides remarkably decreases with plastic flow (Table 3). Therefore, the contribution of MX carbonitrides to the total pinning pressure tends to increase with increasing service temperature, whereas the role of the $M_{23}C_6$ and Laves phases in microstructure stabilization decreases. The higher Zener pinning pressure associated with the $M_{23}C_6$ carbides is attributed to their inhomogeneous distribution and location on the lath boundaries. The detachment of a lath boundary from these particles diminishes the pinning pressure P_L, to almost zero. In contrast, the MX carbonitrides are homogeneously distributed within the metallic matrix. The pinning pressure on lath boundaries exerted by homogeneously distributed particles depends on their size and volume fraction and does not change with the boundary migration rate. Therefore, the MX carbonitrides play an important role for stabilizing the TMLS during creep, in spite of relatively low Zener pinning pressure exerted by these particles. On the other hand, the effect by $M_{23}C_6$ particles is a crucial factor under aging conditions. Precipitates located on the lath boundaries and causing the higher pinning pressure are mostly responsible for the stability of TMLS against aging at elevated temperatures.

5. Conclusions

The tempered martensite lath structure (TMLS) in the 3%Co modified P911 steel that evolved during creep tests at 873 and 923 K was studied in grip and neck portions of crept specimens. The main results are summarized as follows:

1. The TMLS was characterized by two kinds of precipitates, i.e. MX-type carbonitrides with an average size of 30 nm and $M_{23}C_6$-type particles having a size of about 120 nm. The MX particles were homogeneously distributed throughout the martensite structure, whereas the $M_{23}C_6$ particles precipitated at internal boundaries including low-angle lath boundaries.
2. The aging/creep tests were accompanied by the appearance of a Laves phase, which precipitated at high- and low-angle boundaries very similar to $M_{23}C_6$ particles. The size of Laves phase particles was about 170 and 260 nm at 873 K and 923 K, respectively.
3. The TMLS was rather stable during aging; the transverse lath size of 360 nm in the tempered state increased to about 400–500 nm after aging for more than 4000 h. On the other hand, the crept microstructures developed in the neck portions lost their martensite morphology and transformed to a hot worked substructure; the transverse subgrain size was about 660 and 1300 nm after creep at 873 and 923 K, respectively.
4. The boundary precipitates provided effective pinning of grain/lath boundaries in the TMLS. However, the driving force for grain growth rapidly rises with decreasing grain size and may overcome the pinning pressure. The increase of the high-angle boundary spacing during creep tests, therefore, likely resulted

from an accelerated shrinkage of fine grains with sizes less than about 1.5 μm.

5. The pinning pressure acting on the lath boundaries decreased with decreasing misorientation angle. An apparent growth of martensite laths in the grip portions of crept specimens could be associated with the disappearance of low-angle lath boundaries with misorientations less than about 0.5°. Contrary to the grip portions, the substructural parameters evolved in the neck portions were affected by hot working and could hardly be related to the static equilibrium between the driving and pinning pressures.

Acknowledgements

References

[1] F. Masuyama, ISIJ Int. 41 (2001) 612–625.
[2] P.J. Ennis, A. Czyrska-Filemonowicz, Operat. Maint. Mater. (1) (2002) 1–28.
[3] J.C. Vaillant, B. Vandenberghe, B. Hahn, H. Heuser, C. Jochum, Int. J. Pressure Vessels Piping 85 (2008) 38–46.
[4] K. Sawada, M. Takeda, K. Maruyama, R. Ishii, M. Yamada, Y. Nagae, R. Komine, Mater. Sci. Eng. A267 (1999) 19–25.
[5] F. Abe, T. Horiuchi, M. Taneike, K. Sawada, Mater. Sci. Eng. A378 (2004) 299–303.
[6] G. Gupta, G.S. Was, Metall. Mater. Trans. 39A (2008) 150–164.
[7] R.O. Kaybyshev, V.N. Skorobogatykh, I.A. Shchenkova, Phys. Met. Metallogr. 109 (2010) 186–200.
[8] H. Kitahara, R. Ueji, N. Tsuji, Y. Minamino, Acta Mater. 54 (2006) 1279–1288.
[9] F. Abe, M. Taneike, K. Sawada, Int. J. Pressure Vessels Piping 84 (2007) 3–12.
[10] M. Taneike, K. Sawada, F. Abe, Metall. Mater. Trans. 35A (2004) 1255–1261.
[11] P.B. Hirsch, A. Howie, R.B. Nicholson, D.W. Pashley, M.J. Whelan, Electron Microscopy of Thin Crystals, second ed., Krieger, New York, 1977.
[12] K. Suzuki, S. Kumai, H. Kushima, K. Kimura, F. Abe, Tetsu-to-Hagane 86 (2000) 52–59.
[13] A. Gustafson, M. Hattestrand, Mater. Sci. Eng. A333 (2002) 279–286.
[14] O. Prat, J. Garcia, D. Rojas, C. Carrasco, A.R. Kaysser-Pyzalla, Mater. Sci. Eng. A527 (2010) 5976–5983.
[15] Y. Kadoya, B.F. Dyson, M. McLean, Metal. Mater. Trans. A 33 (2002) 2549–2557.
[16] A. Aghajani, Ch. Somsen, G. Eggeler, Acta Mater. 57 (2009) 5093–5106.
[17] S.C. Bose, K. Singh, A.K. Ray, R.N. Ghosh, Mater. Sci. Eng. A476 (2008) 257–266.
[18] C.S. Smith, Trans. A.I.M.E 175 (1948) 15–51.
[19] F.J. Humphreys, M. Hatherly, Recrystallization and Related Annealing Phenomena, second ed., Elsevier, UK, 2004.
[20] W.T. Read, W. Shockley, Phys. Rev. 78 (1950) 275–289.
[21] E. Hornbogen, U. Koster, in: F. Haessner (Ed.), Recrystallization of Metallic Materials, Verlag, Stuttgart, 1978, pp. 159–194.
[22] M.F. Ashby, in: N. Hansen, A.R. Jones, T. Leffers (Eds.), Recrystallization and Grain Growth of Multi-Phase and Particle Containing Materials, RISO, Roskilde, Denmark, 1980, pp. 325–336.
[23] O.D. Sherby, P.M. Burke, Prog. Mater. Sci. 13 (1967) 325–390.
[24] H.J. McQueen, J.J. Jonas, in: R.J. Arsenault (Ed.), Treatise on Materials Science and Technology, Academic Press, New York, 1975, pp. 393–493.
[25] S. Takeuchi, A.S. Argon, J. Mater. Sci. 11 (1976) 1542–1566.
[26] T. Gladman, Proc. Roy. Soc. Lond. 294A (1966) 298–309.
[27] P.M. Hazzledine, P.B. Hirsch, N. Louat, in: N. Hansen, A.R. Jones, T. Leffers (Eds.), Recrystallization and Grain Growth of Multi-Phase and Particle Containing Materials, RISO, Roskilde, Denmark, 1980, pp. 159–164.
[28] P.A. Manohar, M. Ferry, T. Chandra, Iron Steel Inst. Jpn. Int. 38 (1998) 913–924.